Environmental Science and Ecotechnology 16 (2023) 100267

Contents lists available at ScienceDirect

Environmental Science and Ecotechnology

journal homepage: www.journals.elsevier.com/environmental-science-and-ecotechnology/

Original Research

In situ coagulation-electrochemical oxidation of leachate concentrate: A key role of cathodes

Huankai Li [a], Qian Zeng [b], Feixiang Zan [c], Sen Lin [b], Tianwei Hao [a, *]

[a] Department of Civil and Environmental Engineering, Faculty of Science and Technology, University of Macau, Macau, China
[b] Department of Civil and Environmental Engineering, The Hong Kong University of Science and Technology, Clear Water Bay, Hong Kong, China
[c] School of Environmental Science and Engineering, Low-Carbon Water Environment Technology Center (HUST-SUKE), Huazhong University of Science and Technology, Wuhan, China

ARTICLE INFO

Article history:
Received 17 August 2022
Received in revised form
25 February 2023
Accepted 13 March 2023

Keywords:
Leachate concentrate
Electrochemical process
in situ coagulation treatment
Cathode material
Removal mechanism

ABSTRACT

To efficiently remove organic and inorganic pollutants from leachate concentrate, an *in situ* coagulation-electrochemical oxidation (CO-EO) system was proposed using Ti/Ti_4O_7 anode and Al cathode, coupling the "super-Faradaic" dissolution of Al. The system was evaluated in terms of the removal efficiencies of organics, nutrients, and metals, and the underlying cathodic mechanisms were investigated compared with the Ti/RuO_2–IrO_2 and graphite cathode systems. After a 3-h treatment, the Al-cathode system removed 89.0% of COD and 36.3% of total nitrogen (TN). The TN removal was primarily ascribed to the oxidation of both ammonia and organic-N to N_2. In comparison, the Al-cathode system achieved 3–10-fold total phosphorus (TP) (62.6%) and metal removals (>80%) than Ti/RuO_2–IrO_2 and graphite systems. The increased removals of TP and metals were ascribed to the *in situ* coagulation of $Al(OH)_3$, hydroxide precipitation, and electrodeposition. With the reduced scaling on the Al cathode surface, the formation of Al^{3+} and electrified $Al(OH)_3$ lessened the requirement for cathode cleaning and increased the bulk conductivity, resulting in increased instantaneous current production (38.9%) and operating cost efficiencies (48.3 kWh kg_{COD}^{-1}). The present study indicated that the *in situ* CO-EO process could be potentially used for treating persistent wastewater containing high levels of organic and inorganic ions.

1. Introduction

The treatment of leachate concentrate (LC) is gaining worldwide attention, with the LC being a critical component of environmentally friendly waste landfilling or incineration [1,2]. To meet the landfill or incineration leachate discharge standards, membrane processes (e.g., nanofiltration [NF] and reverse osmosis [RO]) are extensively used, resulting in significant amounts of LC (20–30% of the influent leachate) [2,3]. The LC is characterized by a high concentration of refractory organics (e.g., humic substances) and inorganic ions (e.g., heavy metals and nutrients) [3,4] that pose significant risks of contamination to water and soil [5]. More importantly, these contaminants cannot be degraded biologically or via membrane processes (i.e., NF and RO) [6,7]. Hence, a feasible and cost-effective treatment process is required.

Various treatment methods for LC were developed over decades, including physical, physicochemical, electrochemical, and integrated processes. Being good representatives of physicochemical processes, advanced oxidation processes (AOPs) can degrade recalcitrant organics and increase the LC biodegradability via high-efficiency radicals [2,6,8]. However, the ineffectiveness of AOPs in removing inorganics, including phosphate and heavy metals, limits their application [7]. Inorganic ions and dissolved organic matter (DOM) can be effectively removed by electrochemically enhanced AOPs. The high salinity (e.g., chloride ions [Cl^-]) of LC, on the one hand, promotes the electrochemical generation of active chlorine species (ACS) and, on the other hand, reduces the resistance of the bulk liquid [2,8,9]. During the electrochemically enhanced process, phosphate and other inorganics (e.g., heavy metals) are mainly removed by electrocoagulation (EC) or coagulation (CO) [3,4]. However, the EC or CO process does not efficiently remove organics, given that most refractory organics cannot coagulate well. Therefore the integrated process, combining CO or EC with electrochemical oxidation (EO, which can oxidize refractory organics), has

* Corresponding author.
E-mail address: twhao@um.edu.mo (T. Hao).

https://doi.org/10.1016/j.ese.2023.100267

Nomenclature

LC	Leachate concentrate
NF	Nanofiltration
RO	Reverse osmosis
AOP	Advanced oxidation process
DOM	Dissolved organic matters
TAN	Total ammonia
TP	Total phosphorus
EC	Electrocoagulation
EO	Electrochemical oxidation
CO	Coagulation
ACS	Active chlorine species
OH^-	Hydroxyl ion
•OH	Hydroxide radical
Cl^-	Chlorine ion
$Ti/RuO_2–IrO_2$	Ti-based mixed metal oxides of ruthenium and iridium
TDS	Total dissolved solids
BOD_5	5-day biochemical oxygen demand
COD	Chemical oxygen demand
TN	Total nitrogen
$NO_2–N$	Nitrite-N
TCl	Total residual chlorine
$NO_3–N$	Nitrate-N
SEM	Scanning electron microscopy
EDS	Energy dispersive spectrometer
3D-EEM	Three-dimensional excitation-emission matrix
HNO_3	Nitric acid
HCl	Hydrochloric acid
ICE	Instantaneous current efficiency

been developed and evaluated [10]. However, complex construction and costly operation remain the major obstacles to applying the integrated process, although the treatment efficiency is satisfactory.

Efficient electrochemical processes are commonly dependent on electrode materials, which govern the types of reactions and yields of oxidants. The Magneli phase Ti (Ti_nO_{2n-1}, $n = 3–10$) is used extensively as an anode in EO processes to mineralize organics (e.g., humic substances) by yielding hydroxyl radicals (•OH) and ACS, owing to its high oxygen overpotentials and low costs compared with boron-doped diamond [11,12]. As for the cathode, the hydrogen evolution increases pH (hydroxyl ions [OH^-]) during the EO process [1,13]. The pH increase in the cathode vicinity promotes the deposition of co-existing ions and organics on the cathode surfaces, thereby delaying the treatment and reducing the current efficiency by blocking the reaction sites [14]. Interestingly, Al can be dissolved by the OH^- produced at the cathode due to the "super-Faradaic" dissolution resulting from an elevating local pH [15]. The insulating layers can be removed by forming aluminum hydroxide ($Al(OH)_3$) coagulants. Consequently, a better treatment can be achieved by employing Al cathode. Furthermore, the local pH can reach 12, leading to hydroxide flocs forming in the cathode vicinity to coagulate contaminants [16]. The costs of electrodes significantly determine the feasibility of the practical applications. Al, in particular, has low prices and ease of transport given its low density and abundance as a global reserve [17]. Thus, in the present study, it has been hypothesized that using an Al cathode in an electrochemical process combines OH^- to coagulate pollutants, particularly phosphate and heavy metals, and conveys the deposition into the bulk liquid, thereby increasing the current efficiency while maintaining the cost-effectiveness.

The present study aimed to develop a novel *in situ* coagulation-electrochemical oxidation (CO-EO) process for treating LC using an Al cathode. The effectiveness of the CO-EO process was assessed, by comparing it with other cathode systems, in terms of removal efficiencies of organics, nutrients, and metals. Furthermore, the removal mechanisms of the *in situ* CO-EO were investigated with regard to the evolution of organics and nitrogen species and the characterization of cathode surfaces and aluminum precipitates. This novel process can be an alternative method for treating high-saline wastewater with high concentrations of refractory organics and inorganic ions.

2. Materials and methods

2.1. Leachate concentrate and electrodes

Fresh NF and RO LC, collected from a municipal solid waste treatment plant (Kunshan, China), were used in the present study. The NF and RO LC characteristics are provided in Table 1, including their organic, nutrient, metal contents, and total dissolved solids (TDS). The basic characteristics of the electrodes used in the present study are shown in Table S1.

2.2. Setup and operation of the electrochemical process

The electrochemical treatment was carried out in a 1 L single-chamber cell at room temperature (22 ± 1 °C). The Ti/Ti_4O_7 electrode, having a submerged area of 100 cm^2, was selected as the anode due to its strong corrosion resistance, low cost, and concurrently high oxygen overpotential [12]. Al and two common and low-cost electrodes, viz., $Ti/RuO_2–IrO_2$ and graphite, served as cathodes to compare treatment performance; details of the cathodes are summarized in Table S1. The inter-electrode gap was fixed at 1.5 cm, based on preliminary results. To reduce the organic concentration and increase the conductivity, thereby also increasing the electrochemical treatment efficiency, NF-LC and RO-LC were mixed in a 1:1 ratio (v/v), referred to as mixed LC, prior to treatment. The galvanostatic condition (20 mA cm^{-2}) was powered by a direct-current power supply (SS-3020KD, A-BF, Dongguan, China) in accordance with the lifetime and efficiency of Ti/Ti_4O_7 [18] and our preliminary results (Text SI1). Voltages were recorded both before and after sampling. Each batch lasted for 3 h, and a constant magnetic stirring (120 rpm) was implemented throughout the entire experimental period. Samples were periodically taken and filtrated through a 0.45 μm membrane for treatment performance analysis. In the Al-cathode system, samples before and after a 0.45 μm membrane filtration were analyzed to calculate coagulation efficiency. The intact anode was used for each batch experiment.

2.3. Physicochemical analysis

2.3.1. Color and organic analyses

The color of each sample was determined by using the Pt–Co

Table 1
Characteristics of NF and RO leachate concentrate.

Parameter	NF-LC	RO-LC	Metal content (μg L^{-1})	NF-LC	RO-LC
COD (mg L^{-1})	1320 ± 12	155.5 ± 6.4	Fe	3713.7 ± 242.1	783.9 ± 23.4
BOD_5 (mg L^{-1})	75.7 ± 4.3	8.7 ± 3.2	B	5165 ± 156	8552 ± 133
Color (PCU)	3750 ± 50	103.4 ± 4.2	V	46.11 ± 2.7	27.3 ± 1.2
TN (mg L^{-1})	164 ± 3	121 ± 2	Cr	182.7 ± 6.7	33.5 ± 1.2
TP (mg L^{-1})	10.2 ± 0.3	2.4 ± 0.21	Mn	388.7 ± 19.0	533.6 ± 34.3
TAN (mg L^{-1})	38.8 ± 0.5	36.5 ± 0.3	Co	318.9 ± 16.9	81.9 ± 23.1
Nitrate-N (mg L^{-1})	58.8 ± 1.2	78.2 ± 1.1	Ni	1258.8 ± 39.0	70.1 ± 4.6
Nitrite-N (mg L^{-1})	9.5 ± 0.4	12.2 ± 0.3	Cu	17.8 ± 1.4	15.3 ± 2.6
pH	7.8 ± 0.1	8.0 ± 0.3	As	43.0 ± 2.6	37.0 ± 2.2
Cl^- (mg L^{-1})	4340 ± 120	8560 ± 120	Se	5.47 ± 5.0	8.8 ± 4.6
TCl (mg L^{-1})	0.2 ± 0.1	0.1 ± 0.1	Rb	1319.7 ± 46.3	2995.3 ± 168.6
F^- (mg L^{-1})	1.4 ± 0.1	5.6 ± 0.3	Sr	2093.1 ± 89.4	2365.0 ± 134.6
Conductivity (mS cm^{-1})	19.7 ± 0.2	31.8 ± 0.3	Mo	537.3 ± 24.1	5.2 ± 3.4
TDS (g L^{-1})	11.5 ± 0.1	18.3 ± 0.1	Sb	232.7 ± 10.1	3.2 ± 2.1
Na^+ (mg L^{-1})	3163.4 ± 116.6	4238.9 ± 219.1	Pt	N/A	N/A
K^+ (mg L^{-1})	2545.5 ± 81.1	3411.0 ± 164.3	Ba	N/A	N/A
Ca^{2+} (mg L^{-1})	3011.0 ± 139.5	2258.3 ± 124.7	Be	N/A	N/A
Mg^{2+} (mg L^{-1})	1202.4 ± 78.1	400.8 ± 41.3	Se	N/A	N/A
Al (μg L^{-1})	1311.5 ± 121.2	571.3 ± 12.4	Cd	N/A	N/A
Zn (μg L^{-1})	1188.1 ± 96.4	271.9 ± 33.9	Pb	N/A	N/A

N/A: not available.

Standard, and a Portable Colorimeter (M12 (SD), Ruiming, China) set at 455 nm. The dissolved organics of the raw and treated LCs were characterized by using the three-dimensional excitation-emission matrix (3D-EEM) fluorescence spectroscopy with emission (Em) and excitation (Ex) wavelengths ranging between 200–500 and 280–500 nm, respectively (F-4600, Hitachi, Japan). The UV–vis spectra of the mixed LC were acquired by using an ultraviolet-visible-near infrared spectrometer (Shunyu 756 PC, Shanghai, China), with a scan range of 220–600 nm and a scanning interval of 1 nm, to further characterize DOM [19,20]. The E_{300}/E_{400} and E_{250}/E_{365} ratios were used to determine the polymerization degree and molecular weight of organics, including the humification degree of DOM [19].

2.3.2. Organics, nutrients, and inorganic matter analyses

The chemical oxygen demand (COD), total nitrogen (TN), total phosphorus (TP), nitrite (NO_2–N), and total residual chlorine (TCl) concentrations in the mixed LC were determined according to the HACH tests (DR3900, Hach, USA). Cl^- and the 5-day biochemical oxygen demand (BOD_5) were measured by using a digital titrator (HACH, 2063500-CN) and the HACH BOD Trak™ apparatus (II), respectively. Nitrate (NO_3^--N) was measured by ion chromatography (ICS1100 and 900, Dionex, Thermo Fisher Scientific). Total ammonium (TAN) was spectrophotometrically measured with a Nessler reagent by a spectrophotometer (F60722, Lianhua, China) at 425 nm [21].

2.3.3. Metal analyses

High concentrations of Na^+, K^+, Ca^{2+}, and Mg^{2+} were measured by ion chromatography (ICS1100 and 900, Dionex, Thermo Fisher Scientific). Other metal elements, including Al, Cu, Ni, Co, Sr, Zn, Fe, Mn, As, V, Mo, Rb, Se, Cr, Sb, and B, were determined by using the inductively coupled plasma mass spectrometry (ICP-MS, iCAP TQ, Thermo Fisher Scientific) after a 2 h digestion at 180 °C (addition of 7 mL 75% nitric acid [HNO_3] and 1 mL 99% hydrochloric acid [HCl]). All samples were analyzed after acidification with 2% HNO_3. The metal elements without charge include the metal ions complex with organics and free ions with different valences.

2.3.4. Other analyses

The pH, conductivity, and total dissolved solids (TDSs) of all samples were measured by using a portable multimeter (Multi 3420, WTW, Germany). The cathode (Al, Ti/RuO_2–IrO_2, and graphite) surfaces and aluminum precipitate generated in the Al-cathode system were examined by using scanning electron microscopy (SEM) (SU8000, IXRF Inc., US) and an energy dispersive spectrometer (EDS, iXRF Inc., US) after lyophilization (48 h at −50 °C).

2.3.5. Equilibrium modeling

The Visual MINTEQ (version 3.1) was used to evaluate the solubility and equilibrium of the dissolved phases in three electrochemical systems, including all metals, TP, Cl^-, B, and As. The pH of the setup was fixed, based on the final pH of three systems, at 22 °C. The ionic strength to be calculated and Davies approximation for activity correction was selected. Then, the concentrations of all the initially measured ions were entered into the modeling programs to predict the sediments using the "specify possible solid phases" module. The hydroxide and phosphate precipitations, including the existing species of the interesting ions, were provided by the thermodynamic databases in the Visual MINTEQ.

3. Results and discussion

3.1. Color and COD removals

The color of the LC, which is attributed to the refractory humic substances with overlapping chromophores, reached 1867 ± 48 PCU in the mixed LC in the present study. A similar color reduction pattern (from 1867 to 16 PCU) was recorded in these three electrochemical processes (Al, Ti/RuO_2–IrO_2, and graphite-cathode system) (Fig. 1a). Correspondingly, the COD removal efficiencies were higher than 80%, following the pseudo-first-order kinetics ($R^2 > 0.97$), decreasing from 760 ± 40 to 100 ± 32 mg COD L^{-1} (Fig. 1b). The highest COD removal efficiency (89.0%) was obtained in the Al-cathode system. In terms of the COD removal kinetics, the Al-cathode system yielded kinetics ($k_{Al\text{-}obs} = 1.18 \times 10^{-2}$ min^{-1}) approximately 28% higher than the other two systems ($k_{Ti/RuO_2\text{–}IrO_2\text{–}obs} = 0.93 \times 10^{-2}$ min^{-1} and $k_{graphite\text{-}obs} = 0.92 \times 10^{-2}$ min^{-1}). The removals of COD and color can be attributed to the EO of the Ti_4O_7 anode, which generates oxidative species, including hydroxide radical (•OH) and ACS (e.g., Cl_2, HClO, and ClO^-) [2,13].

As shown in Fig. S1, the TCl concentration representing ACS in

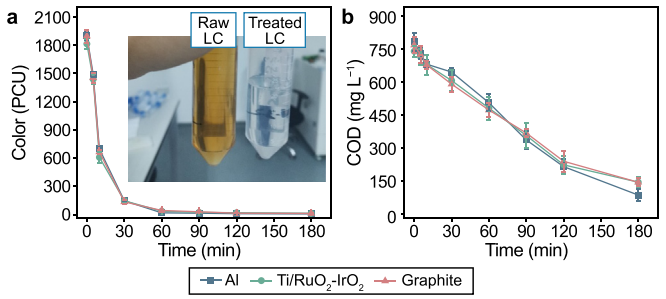

Fig. 1. The color and COD removals of each electrochemical treatment system, with a different cathode, over the treatment period. **a**, $[COD]_0$ = 760 ± 40 mg L^{-1}; **b**, $[color]_0$ = 1867 ± 48 PCU.

these three electrochemical systems reached 2138.8–2423.1 mg L^{-1} after 3 h of treatment. A negative correlation was established between TCl and other parameter concentrations, including Cl^-, COD, and color (Fig. S2). The rapid decreases in color and COD were consistent with the increases in TCl concentration during the first 60 min. Owing to their bleaching properties, ACS, particularly non-radical species (i.e., HClO and ClO^-), facilitate the rapid mineralization and discoloration of DOM [22]. The yield of ACS is dependent on the current density and contact area with the electrode except for anode material [23]; the galvanostatic condition (20 mA cm^{-2}) and same submerged area (100 cm^2) in the present study kept a similar production rate of ACS, which can considerably exceed its consumption rate due to the high Cl^- concentration environment (6426.7 ± 46.2 mg L^{-1}). Thus, the three electrochemical systems performed similarly in terms of COD and color removals, aside from the effectiveness of the cathodes.

3.2. Transformation of organics

The conversion of organics in the mixed LC, before and after treatment, were characterized by 3D-EEM. Humic acids (Em/Ex: >380 nm/>250 nm, intensity of 1521.1 a.u.), fulvic acids (Em/Ex: >380 nm/<250 nm, intensity of 1616.1 a.u.), and soluble microbial by-products (e.g., analogous proteoid phenols) (Em/Ex: 250 < Ex < 400 nm/<380 nm) were dominant in the mixed LC (Fig. 2a) [19]. After 3 h of electrochemical treatment, the intensity of the typical peaks considerably dropped to <200 a.u., namely a blue shift (from top right to bottom left), showing that most refractory humic substances were converted to low-molecular-weight matters (Em/Ex: <380 nm/<250 nm) in the CO-EO systems (Fig. 2b–d).

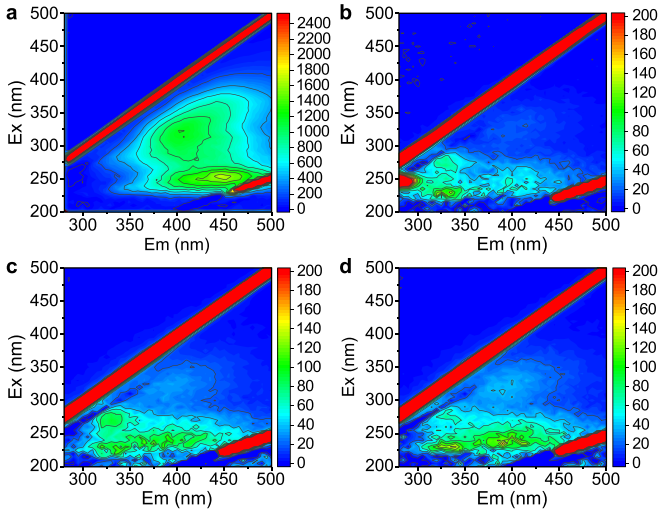

Fig. 2. The 3D-EEM spectrums of the mixed LC before and after electrochemical treatment. **a**, raw mixed-LC; **b**, Al-cathode system; **c**, Ti/RuO$_2$–IrO$_2$-cathode system; **d**, graphite-cathode systems. All samples were diluted 20 folds.

The above results were also validated by the UV/vis spectrum analysis. The strong absorbance at 220–380 nm, particularly E_{254} and E_{280}, which represented the degree of aromatization of organics, rapidly diminished (Fig. S3). The E_{300}/E_{400} and E_{250}/E_{365} ratios increased from 4.6 to between 27.6 and 41.5 and from 4.5 to over 252, respectively, in the three CO-EO systems in the UV–vis spectrum analysis (Table S2). The Al-cathode system displayed the highest E_{300}/E_{400} and E_{250}/E_{365} values, in contrast to those of the Ti/RuO$_2$–IrO$_2$ and graphite cathode systems. Moreover, the BOD_5/COD ratio increased from approximately 0.05 to 0.25, 0.26, and 0.33 in the Al, Ti/RuO$_2$–IrO$_2$, and graphite cathode systems, respectively (Table S3). These results revealed that the organics degraded into DOM with low molecular weight and low degrees of polymerization and coalescence, thereby considerably improving the biodegradability of the mixed LC [19,24]. The improvement of biodegradability of the mixed LC implied that its bio-toxicity and persistent organic concentrations diminished [25,26].

Regarding the persistent organics in the LC, including humic substances, heteroatoms, and benzene, the Ti/Ti_4O_7 anode can theoretically oxidize these organics to aromatic by-products, short-chain aliphatic carboxylic acids (i.e., aldehydes, ketones, and esters), and inorganics (e.g., PO_4^{3-} and NO_3^-), thereby reducing the coalescence and polymerization degrees of the mixed LC [27]. However, the individual EO process is ineffective at decreasing the LC polymerization. For example, aromatic compounds (e.g., benzene) are only partially eliminated by the ACS oxidation [24], which oxidizes the colored groups but does not completely decompose the total organic carbon or mineralize organics [24,28]. At the end of the 3-h treatment, the Al-cathode system yielded a relatively higher COD removal than the other two systems. It was observed that the pH of the Al-cathode system had remained relatively stable throughout the electrochemical treatment, whereas the pH values of the Ti/RuO$_2$–IrO$_2$ and graphite systems both increased from an initial 7.9 to 8.3 ± 0.1 and 8.9 ± 0.1, respectively (Fig. S4). The increase in pH was primarily attributed to the production of OH^- on the cathode [13]. A layer of around 100 μm thickness with a very high pH level (>12) can be created by the *in situ* produced OH^- in the cathode vicinity [29]. The effect of cathode protection failed because the electrons were promptly consumed by cathodic hydrogen evolution. By increasing the local pH, the Al cathode can dissolve, known as a process named "super-Faradaic" dissolution of Al [15]. In an alkaline environment, Al can react with the OH^- generated on the cathode surface to form Al(OH)$_3$ *in situ*, which provides an opportunity to flocculate further or adsorb pollutants. As shown in Fig. S5, the COD removal from the Al(OH)$_3$ coagulants accounted for 14.3–53.1% of the total removal in the Al-cathode system based on the COD concentrations before and after 0.45 μm membrane filtration. As a result, the CO of the Al-cathode system increased the COD removal and considerably decreased the polymerization degree, as observed in the present study.

3.3. Nutrient removal and mechanism

The TP concentrations in the raw mixed LC were 6.6 ± 0.3 mg L^{-1}. After 3 h of treatment, the Al-cathode system yielded 62.6% TP removal, whereas the Ti/RuO$_2$–IrO$_2$ and graphite cathode systems merely removed 22.1% and 18.5% TP, respectively (Fig. 3a). The highest TP removal efficiency in the Al-cathode system can be attributed to the Al(OH)$_3$ coagulants triggered by the Al cathode. The Al concentration increased to a maximum of

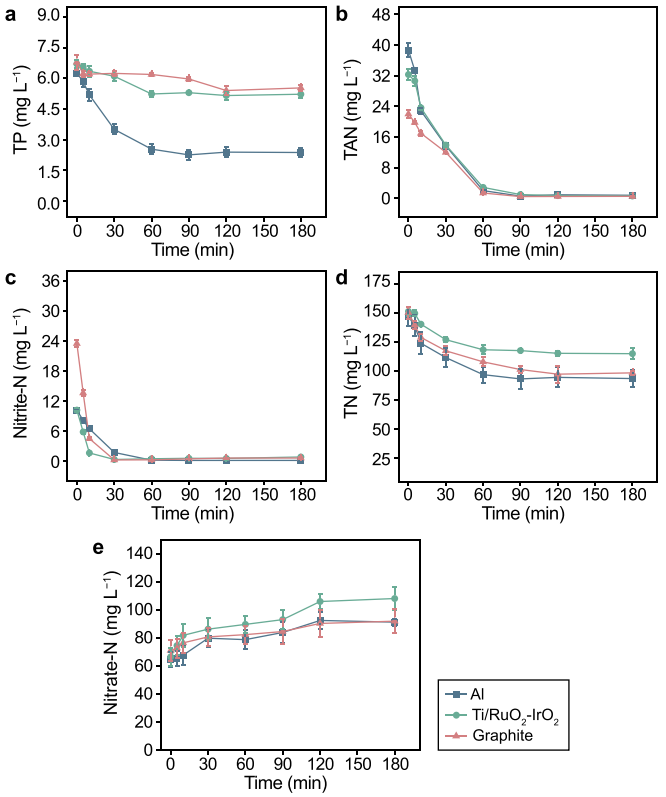

Fig. 3. The nutrient removal of each electrochemical process. **a**, $[TP]_0$ = 6.6 ± 0.3 mg L^{-1}; **b**, $[TAN]_0$ = 31.0 ± 8.4 mg L^{-1}; **c**, $[Nitrite\text{-}N]_0$ = 17.6 ± 7.7 mg L^{-1}; **d**, $[TN]_0$ = 149.6 ± 2.3 mg L^{-1}; **e**, $[Nitrate\text{-}N]_0$ = 67.4 ± 3.3 mg L^{-1}.

3.5 mg L^{-1} after 10 min of operation (Fig. S6), and there was insignificant TP removal at the condition without filtration. The released Al^{3+} and pH (~8.5) condition facilitated the precipitation of $Al_3(OH)_3(PO_4)_2$, which were adsorbed onto positively charged aluminum hydroxide flocculants or acted as centers of precipitation for aluminum hydrolysis [30,31]. Furthermore, in the three cathode systems with a high Ca^{2+} concentration (2634.6 ± 117.9 mg L^{-1}), TP can be removed via the formations of amorphous calcium phosphate ($Ca_3(PO_4)_2$) and $Ca_5(PO_4)_3(OH)$, particularly when the pH increased [16]. Of the three cathode systems, the pH of the Al-cathode system was the lowest, hence the formations of ($Ca_3(PO_4)_2$) and $Ca_5(PO_4)_3(OH)$ were minimal. The TP removal can also be affected by the Cl^- ions. In particular, $Al(OH)_3$ can react with Cl^- (equations (1)–(4)) and OH^- to produce $AlCl_4^-$ and AlO_2^-, respectively [32], which deteriorates the $Al(OH)_3$ formation [33]. However, based on the effectiveness of the three systems at removing TP and Ca^{2+}, Cl^- did not play a dominant role.

$$Al(OH)_3 + Cl^- \rightarrow Al(OH)_2Cl + OH^- \quad (1)$$

$$Al(OH)_2Cl + Cl^- \rightarrow Al(OH)\,Cl_2 + OH^- \quad (2)$$

$$Al(OH)Cl_2 + Cl^- \rightarrow AlCl_3 + OH^- \quad (3)$$

$$AlCl_3 + Cl^- \rightarrow AlCl_4^- \quad (4)$$

In the LC, nitrogen mainly consists of organic nitrogen (organic-N), nitrate, and TAN. TAN and nitrite comprised 28.1–33.2% of TN and fluctuated between 22.0 and 38.7 mg L^{-1} and 10.2–23.5 mg L^{-1}, respectively. The rapid decreases in TAN and nitrite were recorded during the first 60 min of treatment in all electrochemical processes (Fig. 3b and c), as expected in the oxidation system (equations (5)–(8)) [34]. Based on the stoichiometry of ammonia oxidation (equations (5)–(6)), 2–3 mol protons are produced for 1-mol ammonia-N oxidation. Thus, after 30 min of TAN oxidation, up to 3.6–5.4 mM H^+ can be generated on the anode. This explained the decrease in pH during the first 30 min of treatment (Fig. S4).

$$NH_4^+ + ClO^- \rightarrow 0.5N_2 + H_2O + 2H^+ + Cl^- \quad (5)$$

$$MO_x(\bullet OH) + NH_4^+ \rightarrow MO_x + 0.5N_2 + H_2O + 3H^+ \quad (6)$$

$$ClO^- + 2NO_2^- + OH^- \rightarrow 2NO_3^- + Cl^- + H^+ \quad (7)$$

$$MO_x(\bullet OH) + NO_2^- \rightarrow MO_x + NO_3^- + OH^- \quad (8)$$

Overall, between 24.0 and 36.3% of TN were removed in the present study (Fig. 3d), which can be attributed to the partial TAN oxidation into nitrogen gas (N_2) [3]. In the presence of •OH and ACS, TAN can be converted to N_2 and/or nitrate (equations (5), (6), and (9)), while ACS oxidizes TAN to N_2, rather than nitrate, in the presence of a high concentration of Cl^- [34]. Nevertheless, all the TAN (average concentration of 31.0 ± 8.4 mg L^{-1}) oxidized to N_2 merely accounted for 14.6–26.3% of the TN removal. Moreover, the nitrite was completely oxidized to nitrate (Fig. 3c), resulting in a zero net nitrogen removal. Thus, the degradation of the organic nitrogen to TAN (equation (10)), and subsequent oxidation to N_2 in the presence of oxidants, probably contributed to the additional TN removal in these three systems.

$$NH_4^+ + 4ClO^- \rightarrow NO_3^- + H_2O + 2H^+ + 4Cl^- \quad (9)$$

$$\text{Organic-N} + \bullet OH/ClO^- \rightarrow NH_4^+ + H_2O + H^+ + Cl^- \quad (10)$$

The fates of the different nitrogen species were further examined in the three electrochemical systems, where N_2 was determined based on the nitrogen balance (assuming zero NO_2 and N_2O productions), as shown in Fig. 4. Organic-N, accounting for ~24.4% (33.5–42.4 mg L^{-1}) in the mixed LC, was converted to TAN, and subsequently to N_2 and nitrate (equations (5), (6), (9) and (10)) [34,35], which accounted for over 61% and 24% of TN, respectively, at the end of the test. After 3 h of treatment, the Al and Ti/RuO_2–IrO_2 cathode systems showed the lowest and highest organic-N concentrations, respectively, consistent with the CO effects of $Al(OH)_3$ on organic removal (Figs. 1b, 2, and S3). Nitrate can be reduced to TAN and NO_2^- by accepting electrons from the cathode, and the resulting NO_2^- can further be reduced to N_2 (equations (11)–(14)) [36]. Theoretically, the reduction rate of nitrate-N is much slower than the oxidation rate of nitrite-N in the presence of TCl and Cl^- [37]. Yet, in the present study, the increase rates of nitrate-N of 0.7 and 0.2 mg L^{-1} min^{-1}) were much slower than the decrease rates of nitrite-N of 1.8 and 0.4 mg L^{-1} min^{-1}), respectively, in the graphite and Al cathode systems, during the first 5 min. This suggested the occurrence of nitrate reduction in the systems. However, at the end of the treatment, the nitrate concentration in the three cathode systems increased marginally due to the removal of nitrite and organic-N (Figs. 3e and 4). This can be explained by the high Cl^- concentration in the mixed LC that can reduce the available reaction surface area for nitrate reduction on the cathode via the Cl^- specific adsorption [38].

$$NO_3^- + H_2O + 2e^- \rightarrow NO_2^- + 2OH^- \quad (11)$$

$$NO_3^- + 6H_2O + 8e^- \rightarrow NH_3 + 9OH^- \quad (12)$$

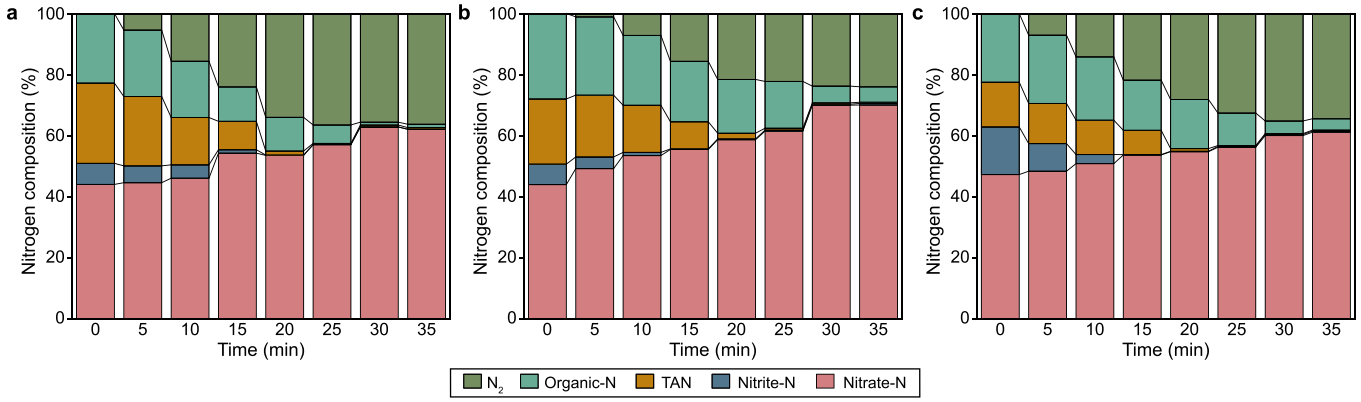

Fig. 4. The evolution of the nitrogen species for the three cathode systems. **a**, Al-cathode system; **b**, Ti/RuO_2–IrO_2-cathode system; **c**, graphite-cathode system.

$$NO_3^- + 5H_2O + 6e^- \rightarrow NH_3 + 7OH^- \quad (13)$$

$$NO_2^- + 2H_2O + 3e^- \rightarrow 0.5N_2 + 4OH^- \quad (14)$$

3.4. Metal removal and mechanism

The raw mixed LC contained a variety of metals, including high concentrations (761–3820 mg L^{-1}) of light metals, including Na^+, K^+, Ca^{2+}, and Mg^{2+}, and minute concentrations (14–730 μg L^{-1}) of heavy metals, including Cu, Ni, Co, Sr, Mo, Zn, Fe, Mn, As, Sb, and Cr. Ni, Sr, Zn, Fe, Mn, Cu, and V can cause abnormal cholesterol metabolism, hyperthyroidism, poisoning, and cancer, among others, even in low concentrations (0.003–2 mg L^{-1}) [39,40]. Therefore, their removal is a matter of great concern. The metal removal efficiencies and concentration changes in the three electrochemical systems are presented in Table 2 and Figs. 5 and S7, respectively. The removal efficiencies of 3.3–8.5%, 1.6–21.4%, 11.3–12.6%, and 13.9–22.2% were obtained for Na^+, K^+, Ca^{2+}, and Mg^{2+}, respectively. The Al-cathode system yielded the highest removal efficiencies for Na^+, K^+, Ca^{2+}, Mg^{2+}, Cu, Ni, Co, Sr, Zn, Fe, Cr, Mo, Mn, As, and V. This can be attributed to the adsorption of aluminum hydroxide species triggered by the cathodic Al dissolution, as was described in Section 3.2. A 36.2% increase in the Al^{3+} concentration was recorded in the Al-cathode system after 3 h of treatment, whereas 17.4% and 41.4% of Al were removed by the Ti/RuO_2–IrO_2 and graphite cathode systems, respectively.

The pH affects the formation and CO capabilities of $Al(OH)_3$ and metal hydroxides. Produced OH^- at the cathode can instantly be consumed to form $Al(OH)_3$, given the small K_{sp} of $Al(OH)_3$ of 1.3×10^{-33} [16,41]. Presumably, all produced OH^- reacts with the Al cathode, and the theoretical dissolved Al concentration could reach 3326.3 mg L^{-1}, which is much lower than the produced aluminum precipitate (presumably $Al[OH]_3$) concentration of 6985.4 mg Al L^{-1} after 3 h of treatment (Text SI2). The increased Al dissolution revealed the existence of cathodic corrosion (pitting) caused by the high concentration of ACS and Cl^- [33,42]. And hence, the Ti_4O_7-based anodic oxidation could improve the CO of the Al cathode, forming a synergistic system. Owing to the amphoteric characteristic of aluminum and aluminum hydroxides, the nearly neutral resulting pH ranging 7–9 renders the aluminum hydroxides anionic, thereby making them more receptive to metal cations than anions [43]. However, in the other two systems, the gradual increase in pH can lead to metal hydroxide precipitations. As shown in Fig. 5, the concentrations of Zn, Fe, Cu, Ni, Co, Sr, and Mo showed marginal variations during the first 30 min and rapid decreases during the later stages. It is suggested that their removals are partially due to metal hydroxide precipitations, given that the pH marginally decreased between 0 and 30 min due to TAN oxidation (Fig. S4).

To identify the contribution of metal precipitations to metal removals, Visual MINTEQ was used to simulate the system precipitations (Tables S4–S6). It is worth noting that only Fe^{3+} and phosphate were predicted to precipitate wholly in all three systems. Ni^{2+} or Zn^{2+} precipitated, only in the Ti/RuO_2–IrO_2 and graphite cathode systems, via the formation of hydroxide sediments (i.e., $Ni[OH]_2$(c) and $Zn[OH]_2$[epsilon]). Ca^{2+} and V^{3+} displayed precipitation rates of 1.4–1.6% and 10.8–20.2%, respectively; their respective proportions of the total removals were 6.1% and 11.9%. As expected, the precipitation ratios of the aforementioned metals (Ca^{2+}, V^{3+}, Ni^{2+}, and Zn^{2+}) increased with pH from the Al-cathode to the graphite-cathode system.

Table 2
The removal efficiencies of metals after 3 h of treatment in the three electrochemical process systems.

Metal	Removal efficiency (%)			Metal	Removal efficiency (%)		
	Al	Ti/RuO_2–IrO_2	Graphite		Al	Ti/RuO_2–IrO_2	Graphite
Cu	93.5	21.7	29.9	Mn	98.9	64.6	67.1
Ni	84.1	7.8	13.9	As	69.4	7.3	20.4
Co	33.7	25.5	24.9	V	90.5	12.9	15.4
Sr	81.8	16.7	49.7	Na^+	8.5	3.3	0.8
Zn	67.7	24.2	32.0	K^+	21.4	2.4	1.6
Fe	83.5	64.2	68.6	Ca^{2+}	22.2	21.9	13.9
Mo	49.0	18.5	19.9	Mg^{2+}	12.6	11.3	12.4
Cr	47.0	2.3	39.3				

3.5. Electrodeposition and aluminum precipitate

Apart from the precipitation and adsorption of aluminum hydroxides, electrodeposition can also contribute to metal removal via a deposition process combining metals and single or multiple inorganic ions (e.g., Cl^-, CO_3^{2-}, PO_4^{3-}, OH^-, etc.) on the cathode surface. In particular, this phenomenon can be improved by producing OH^- on the cathode surface [16]. The electrodeposition on three cathodes and aluminum precipitate produced in the Al-cathode system were studied by the SEM and EDS analyses (Fig. 6) to investigate the removal mechanisms of metals and nutrients. On the Al, Ti/RuO_2–IrO_2, and graphite cathode surfaces, sediments resembling snowflakes and pellets were observed from the SEM analyses (Fig. 6a–c). The aluminum precipitate produced

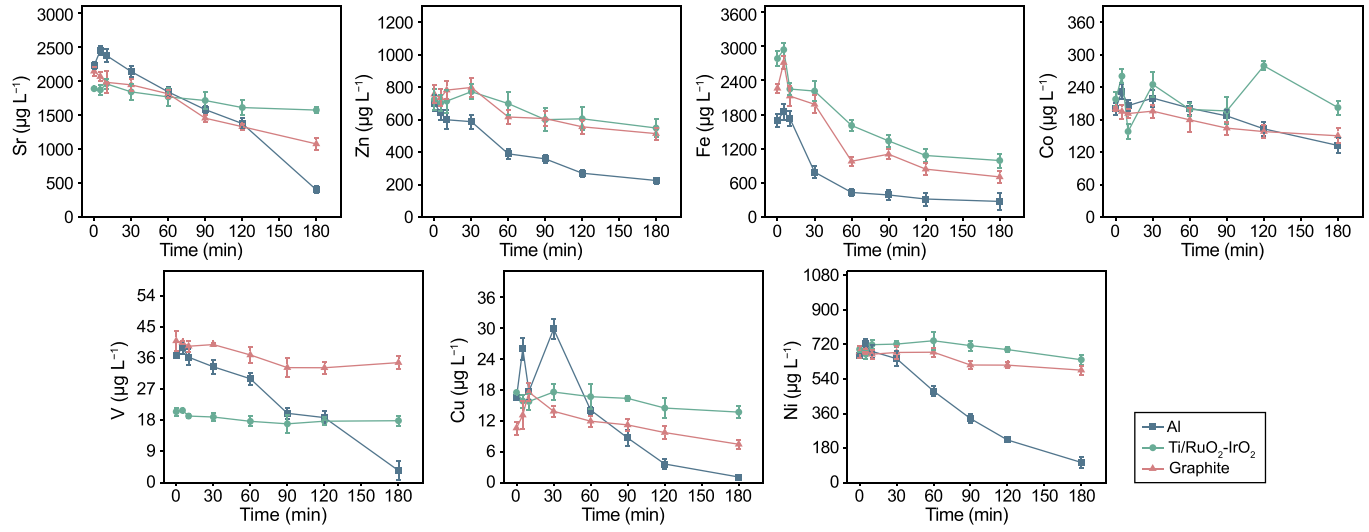

Fig. 5. The pH-dependent metal removal for all three electrochemical systems.

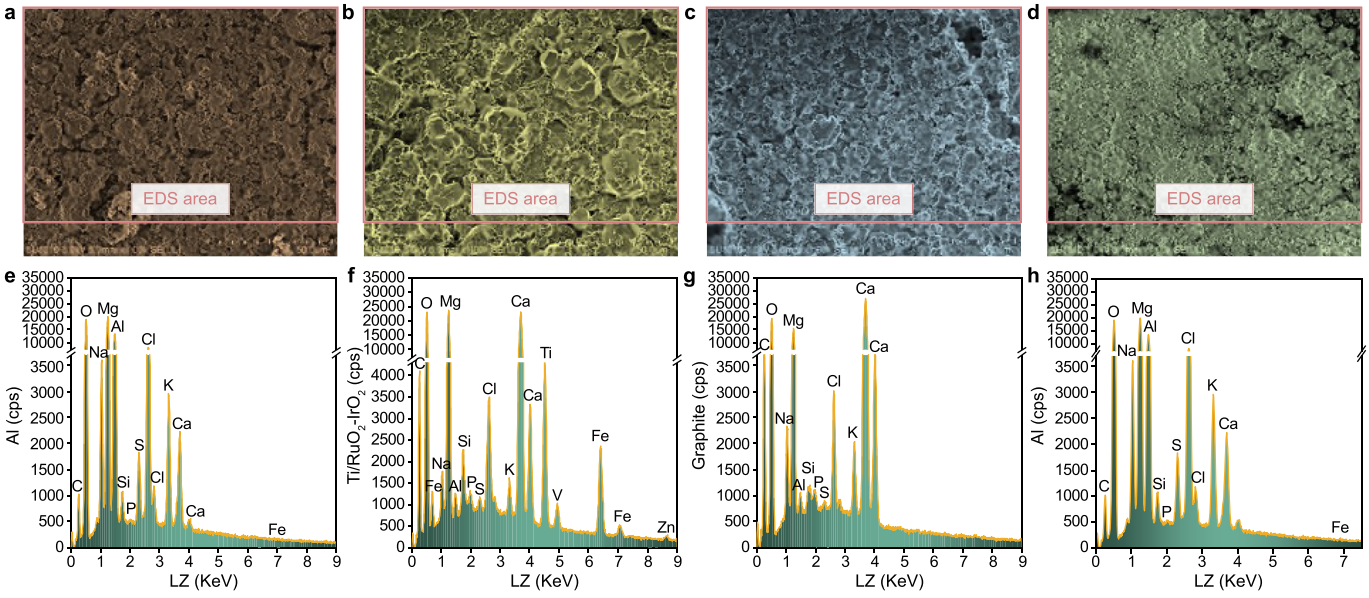

Fig. 6. The SEM-EDS analyses of the three cathode surfaces and aluminum precipitate after 3 h of treatment. **a**–**d**, For SEM: Al (**a**); Ti/RuO_2–IrO_2 (**b**); graphite (**c**); and aluminum precipitate (**d**). **e**–**f**, For EDS: Al (**e**); Ti/RuO_2–IrO_2 (**f**); graphite (**g**); and aluminum precipitate (**h**).

in the Al-cathode system appeared like cotton wool and gel (Fig. 6d). Also, the aluminum precipitate had a comparatively fragile and porous structure in contrast with that produced by chemical CO [43]. The treated mixed LC can be separated from the aluminum precipitate, in a sediment tank, before being discharged. Fewer sediments emerged on the Al cathode surface than the Ti/RuO_2–IrO_2 and graphite cathode surfaces. Given that Al is amphoteric, it dissolved with the sediments into the mixed LC, thus reducing the requirement for cathode cleaning and improving the instantaneous current efficiency (Text SI3) [44].

The EDS spectrums were further performed to characterize the depositions and precipitates. As shown in Fig. 6e–h and Table S7, heavy metals, including Zn, Fe, Cu, Mn, Co, and Ni, among others, attached themselves to the three cathodes and aluminum precipitate, thereby confirming the contribution of electrodeposition and CO to the removals of metals. The intensities of Na^+ and K^+ in the EDS spectrum of the aluminum precipitate were more significant than the intensities of the three cathode surfaces. Concerning electrodeposition, the higher pH in the graphite-cathode could facilitate the formation of metal hydroxides, which can adsorb metals like the $Al(OH)_3$ flocs. Nevertheless, the Ti/RuO_2–IrO_2 cathode exhibited greater electrodeposition than the other two cathodes, particularly the rhombohedral-shaped crystals (Fig. 6b), which incorporated more Ca^{2+}, Mg^{2+}, and Na^+ as determined by SEM-EDS analysis [16,45]. The removal of high concentrations of fractions (Na, K, Ca, and Mg) implies that the Al-cathode system aided in the desalination of the LC. This is also supported by the changes in TDSs; it decreased from 15.1 ± 0.2 to 13.8 g L^{-1} (Fig. S8a), resulting in a desalination rate of 9.2% after separating the $Al(OH)_3$ flocculants from the treated LC. In addition to metals, other inorganic ions, including PO_4^{3-} and Cl^-, coagulated in the aluminum precipitate (Table S7). In an electrical field, the PO_4^{3-} and Cl^- anions

gravitate toward the anode rather than the cathode. Thus, their presence implies that insulating sediments, including $AlCl_3$ (equations (3)–(6)), $Ca_3(PO_4)_2$, and $Ca_5(PO_4)_3(OH)$, among others, can form on the cathode surfaces in high concentrations of Ca^{2+} (2634.6 ± 117.9 mg L^{-1}) and Cl^- (6177.8 ± 276.6 mg L^{-1}) [16,32,46]. However, due to the difficult formation of the insoluble nitrogen-related sediments and electrostatic repulsion between nitrate and aluminum precipitate [47,48], the TN removal was merely defined by the TAN oxidation to N_2, nitrate reduction and organic-N oxidation.

3.6. Environmental implications

The *in situ* CO-EO treatment is effective at simultaneously removing organics (i.e., humic substances and color) and inorganics (i.e., nutrients and metals) from the LC. The sludge volume index (SVI) of the CO-aluminum precipitate was approximately 200 mL g^{-1}, similar to the flocs produced by aluminum-anode EC and municipal wastewater treatment plants [43]. It is therefore easy to separate and dewater the pollutants from the treated LC. Using the acid digestion method, the removed metals can be further precipitated and/or recovered [49]. More importantly, based on the experimental and literature data analyses, the energy consumption of the *in situ* CO-EO process can be approximately 48.3 kWh kg_{COD}^{-1}, about 50% of that of the previous study [50]. On the one hand, the low scaling on the Al cathode surface, in particular, lessened the requirement for cathode cleaning in the EO process due to the Al cathode dissolution (Fig. 6); the Al^{3+} dissolution, and the formation of electrified aluminum hydroxides, can further reduce the resistance of bulk liquid (Fig. S8c), lower the energy consumption, and improve the current efficiency. Compared to the mono-electrochemical process, which generally requires 6–8 h for treatment, the CO-EO system could achieve comparable results in 3 h [51]. On the other hand, although the cathode dissolution consumes Al, shortening the operating life of the cathode, the Al cathode is one of the cheapest electrodes used in electrochemical systems, particularly when compared with other cathodes in the electro-Fenton process [52] (Text SI4). In view of the electrochemical process and removal of inorganic ions, the EC is conventionally introduced to remove organic and inorganic pollutants via the Al anode dissolution. Meanwhile, the high concentration of Cl^- in the mixed LC can remove the cathode passivation in the process; this can increase current efficiency and Al cathode dissolution when Al is used as the cathode [7,22]. Hence, the cathode dissolution in the present study solved the electrodeposition of the EO process and integrated the CO and EO processes, reaching higher removal efficiencies for TP and metals. However, the sustainability and applicability of the *in situ* CO-EO treatment demand long-term validation.

The current study suggests that the *in situ* CO-EO process equipped with Al cathode mostly applies to bio-refractory wastewaters containing high concentrations of organic and inorganic pollutants, particularly those with high Cl^- concentration. Thus, the treatment subsequent to the CO-EO process can have lower costs, given the resulting higher removal efficiency of pollutants, particularly TP and metals, at the same BOD level. Also, regardless of the initial pH of wastewater, the Al cathode and generated $Al(OH)_3$, including the formed oxidation film (Al_2O_3) on the Al cathode surface, can act as a buffer maintaining the pH between 7 and 9 (Fig. S4) [33,47]. Besides, in an alkaline environment, organic-N and TAN are mainly converted to N_2, rather than nitrate, via the TCl oxidation, thereby enhancing the TN removal [5]. Nevertheless, the excessive TCl can induce corrosion of parts of the reactors (i.e., reaction tanks and cables) and form chloride by-products, which is necessary to be considered in real-world applications. Hence, as per the results of the present study, using the mixture of raw LC and short-time LC to reduce the corrosion of TCl and the concentration of bio-refractory organics is probable.

4. Conclusion

Three electrochemical systems for the mixed LC treatment were investigated in the present study. Among the three systems, the Al-cathode system, incorporating the Ti/Ti_4O_7 anode (*in situ* CO-EO), displayed the best removal efficiency because of the "super-Faradaic" dissolution of the Al cathode. COD, TP, TAN, nitrite, organic-N, and metals were successfully removed from the mixed LC via *in situ* oxidation and CO. Due to the difficulty of nitrate to be removed via CO and electrodeposition, the TN removal was merely attributed to the oxidation of TAN and organic-N to N_2. The *in situ* CO, hydroxide precipitation, and electrodeposition promoted the removal of inorganic ions, including TP and metals. The low scaling on the Al cathode surface, the formation of the aluminum precipitate, Al^{3+}, and electrified aluminum hydroxides, lessened the requirement for cathode cleaning and increased the bulk conductivity in the EO process to enhance the instantaneous current production (38.9%) and operating cost efficiencies (48.3 kWh kg_{COD}^{-1}). Prior to scaling up, detailed operation and impact studies of high TCl and nitrate concentrations should be conducted to maximize the treatment efficiency and minimize the operating costs.

CRediT author contribution statement

Huankai Li: Data curation, Writing - Original draft, Methodology. **Qian Zeng:** Conceptualization, Writing - Review & Editing. **Feixiang Zan:** Writing - Review & Editing. **Sen Lin:** Visualization, Writing - Review & Editing. **Tianwei Hao:** Conceptualization, Writing - Review & Editing, Supervision.

Declaration of competing interest

The authors declare that they have no known competing financial interests or personal relationships that could have appeared to influence the work reported in this paper.

Acknowledgment

This research was supported by the Science and Technology Development Fund of Macau (No. 0002/2019/AGJ & 0104/2018/A3) and the Research Committee of the University of Macau Project (No. MYRG2019-00045-FST & MYRG2020-00148-FST).

Appendix A. Supplementary data

Supplementary data to this article can be found online at https://doi.org/10.1016/j.ese.2023.100267.

References

[1] S. Top, E. Sekman, S. Hoşver, M.S. Bilgili, Characterization and electrocaogulative treatment of nanofiltration concentrate of a full-scale landfill leachate treatment plant, Desalination 268 (1–3) (2011) 158–162.
[2] Y. Cui, W. Xue, S. Yang, J. Tu, X. Guo, Z. Liu, Electrochemical/peroxydisulfate/Fe^{3+} treatment of landfill leachate nanofiltration concentrate after ultrafiltration, Chem. Eng. J. 353 (2018) 208–217.
[3] H. Chang, R. Hu, Y. Zou, X. Quan, N. Zhong, S. Zhao, Y. Sun, Highly efficient reverse osmosis concentrate remediation by microalgae for biolipid production assisted with electrooxidation, Water Res. 174 (2020), 115642.
[4] D. Chu, Z.L. Ye, S. Chen, Interactions among low-molecular-weight organics, heavy metals, and Fe (III) during coagulation of landfill leachate nanofiltration concentrate, Waste Manage. (Tucson, Ariz.) 104 (2020) 51–59.
[5] A. Fernandes, M. Pacheco, L. Ciríaco, A. Lopes, Review on the electrochemical processes for the treatment of sanitary landfill leachates: present and future,

Appl. Catal. B Environ. 176 (2015) 183–200.
[6] H. Wang, X. Li, Z. Hao, Y. Sun, Y.-n. Wang, W. Li, Y.F. Tsang, Transformation of dissolved organic matter in concentrated leachate from nanofiltration during ozone-based oxidation processes (O_3, O_3/H_2O_2 and O_3/UV), J. Environ. Manag. 191 (2017) 244–251.
[7] H. Li, H. Liu, Treatment and recovery methods for leachate concentrate from landfill and incineration: a state-of-the-art review, J. Clean. Prod. 329 (2021), 129720.
[8] L. Labiadh, A. Fernandes, L. Ciríaco, M.J. Pacheco, A. Gadri, S. Ammar, A. Lopes, Electrochemical treatment of concentrate from reverse osmosis of sanitary landfill leachate, J. Environ. Manag. 181 (2016) 515–521.
[9] Z. Zhang, C. Teng, K. Zhou, C. Peng, W. Chen, Degradation characteristics of dissolved organic matter in nanofiltration concentrated landfill leachate during electrocatalytic oxidation, Chemosphere (2020), 127055.
[10] G.S. Soomro, C. Qu, N. Ren, S. Meng, X. Li, D. Liang, S. Zhang, Y. Li, Efficient removal of refractory organics in landfill leachate concentrates by electro-coagulation in tandem with simultaneous electro-oxidation and in-situ per-oxone, Environ. Res. 183 (2020), 109249.
[11] P. Geng, G. Chen, Antifouling ceramic membrane electrode modified by Magnéli Ti_4O_7 for electro-microfiltration of humic acid, Sep. Purif. Technol. 185 (2017) 61–71.
[12] H. Lin, J. Niu, S. Liang, C. Wang, Y. Wang, F. Jin, Q. Luo, Q. Huang, Development of macroporous Magnéli phase Ti_4O_7 ceramic materials: as an efficient anode for mineralization of poly-and perfluoroalkyl substances, Chem. Eng. J. 354 (2018) 1058–1067.
[13] S. You, B. Liu, Y. Gao, Y. Wang, C.Y. Tang, Y. Huang, N. Ren, Monolithic porous Magnéli-phase Ti_4O_7 for electro-oxidation treatment of industrial wastewater, Electrochim. Acta 214 (2016) 326–335.
[14] I. Berkani, M. Belkacem, M. Trari, F. Lapicque, K. Bensadok, Assessment of electrocoagulation based on nitrate removal, for treating and recycling the Saharan groundwater desalination reverse osmosis concentrate for a sustainable management of Albien resource, J. Environ. Chem. Eng. 7 (2) (2019), 102951.
[15] M. Mechelhoff, G.H. Kelsall, N.J.D. Graham, Electrochemical behaviour of aluminium in electrocoagulation processes, Chem. Eng. Sci. 95 (2013) 301–312.
[16] Y. Lei, B. Song, R.D. van der Weijden, M. Saakes, C.J.N. Buisman, Electrochemical induced calcium phosphate precipitation: importance of local pH, Environ. Sci. Technol. 51 (19) (2017) 11156–11164.
[17] M.Y.A. Mollah, J.A.G. Gomes, K.K. Das, D.L. Cocke, Electrochemical treatment of Orange II dye solution—use of aluminum sacrificial electrodes and floc characterization, J. Hazard Mater. 174 (1–3) (2010) 851–858.
[18] P.C.S. Hayfield, Development of a New Material: Monolithic Ti_4O_7 Ebonex Ceramic, Royal Society of Chemistry, 2007.
[19] M. Chen, Y. He, Z. Gu, Microwave irradiation activated persulfate and hydrogen peroxide for the treatment of mature landfill leachate effluent from a membrane bioreactor, Sep. Purif. Technol. (2020), 117111.
[20] A. Zhang, Z. Gu, W. Chen, Q. Li, G. Jiang, Removal of refractory organic pollutants in reverse-osmosis concentrated leachate by Microwave–Fenton process, Environ. Sci. Pollut. Res. 25 (29) (2018) 28907–28916.
[21] A. Apha, Standard Methods for the Examination of Water and Wastewater, 23rd, Water Environment Federation, American Public Health Association, American, 2017.
[22] C.A. Martinez-Huitle, M.A. Rodrigo, I. Sires, O. Scialdone, Single and coupled electrochemical processes and reactors for the abatement of organic water pollutants: a critical review, Chem. Rev. 115 (24) (2015) 13362–13407.
[23] K. Cho, Y. Qu, D. Kwon, H. Zhang, C.A. Cid, A. Aryanfar, M.R. Hoffmann, Effects of anodic potential and chloride ion on overall reactivity in electrochemical reactors designed for solar-powered wastewater treatment, Environ. Sci. Technol. 48 (4) (2014) 2377–2384.
[24] H. Wang, D. Ge, Z. Cheng, N. Zhu, H. Yuan, Z. Lou, Improved understanding of dissolved organic matter transformation in concentrated leachate induced by hydroxyl radicals and reactive chlorine species, J. Hazard Mater. 387 (2020), 121702.
[25] M. El Kateb, C. Trellu, A. Darwich, M. Rivallin, M. Bechelany, S. Nagarajan, S. Lacour, N. Bellakhal, G. Lesage, M. Héran, Electrochemical advanced oxidation processes using novel electrode materials for mineralization and biodegradability enhancement of nanofiltration concentrate of landfill leachates, Water Res. 162 (2019) 446–455.
[26] Y. Wang, C. Zhou, G. Meng, J. Bai, X. Geng, L.V. Yanli, X. Chen, Treatment of landfill leachate membrane filtration concentrate by synergistic effect of electrocatalysis and electro-Fenton, J. Water Process Eng. 37 (2020), 101458.
[27] S.O. Ganiyu, N. Oturan, S. Raffy, M. Cretin, R. Esmilaire, E. van Hullebusch, G. Esposito, M.A. Oturan, Sub-stoichiometric titanium oxide (Ti4O7) as a suitable ceramic anode for electrooxidation of organic pollutants: a case study of kinetics, mineralization and toxicity assessment of amoxicillin, Water Res. 106 (2016) 171–182.
[28] S. Song, J. Fan, Z. He, L. Zhan, Z. Liu, J. Chen, X. Xu, Electrochemical degradation of azo dye CI Reactive Red 195 by anodic oxidation on Ti/SnO2–Sb/PbO2 electrodes, Electrochim. Acta 55 (11) (2010) 3606–3613.
[29] Y. Li, D. Lu, X. Liu, Z. Li, H. Zhu, J. Cui, H. Zhang, X. Mao, Coupling of cathodic aluminum dissolution and anodic oxidation process for simultaneous removal of phosphate and ammonia in wastewaters, Chem. Eng. J. 427 (2022), 130944.
[30] P.I. Omwene, M. Kobya, Treatment of domestic wastewater phosphate by electrocoagulation using Fe and Al electrodes: a comparative study, Process Saf. Environ. 116 (2018) 34–51.
[31] L.P. Zini, M. Longhi, E. Jonko, M. Giovanela, Treatment of automotive industry wastewater by electrocoagulation using commercial aluminum electrodes, Process Saf. Environ. 142 (2020) 272–284.
[32] K. Mansouri, K. Ibrik, N. Bensalah, A. Abdel-Wahab, Anodic dissolution of pure Aluminum during electrocoagulation process: influence of supporting electrolyte, initial pH, and current density, Ind. Eng. Chem. Res. 50 (23) (2011) 13362–13372.
[33] G. Mouedhen, M. Feki, M.D.P. Wery, H.F. Ayedi, Behavior of aluminum electrodes in electrocoagulation process, J. Hazard Mater. 150 (1) (2008) 124–135.
[34] G. Pérez, J. Saiz, R. Ibañez, A.M. Urtiaga, I. Ortiz, Assessment of the formation of inorganic oxidation by-products during the electrocatalytic treatment of ammonium from landfill leachates, Water Res. 46 (8) (2012) 2579–2590.
[35] H. Feng, Z. Chen, X. Wang, S. Chen, J. Crittenden, Electrochemical advanced oxidation for treating ultrafiltration effluent of a landfill leachate system: impacts of organics and inorganics and economic evaluation, Chem. Eng. J. (2020), 127492.
[36] B.P. Dash, S. Chaudhari, Electrochemical denitrificaton of simulated ground water, Water Res. 39 (17) (2005) 4065–4072.
[37] G. Pérez, R. Ibáñez, A.M. Urtiaga, I. Ortiz, Kinetic study of the simultaneous electrochemical removal of aqueous nitrogen compounds using BDD electrodes, Chem. Eng. J. 197 (2012) 475–482.
[38] M. Li, C. Feng, Z. Zhang, N. Sugiura, Efficient electrochemical reduction of nitrate to nitrogen using Ti/IrO2–Pt anode and different cathodes, Electrochim. Acta 54 (20) (2009) 4600–4606.
[39] A. Pal, J. Jayamani, R. Prasad, An urgent need to reassess the safe levels of copper in the drinking water: lessons from studies on healthy animals harboring no genetic deficits, Neurotoxicology 44 (2014) 58–60.
[40] U.C. Nkwunonwo, P.O. Odika, N.I. Onyia, A review of the health implications of heavy metals in food chain in Nigeria, Sci. World J. 2020 (2020) 6594109.
[41] S. Wang, Q. Wang, Experimental studies on pretreatment process of brackish water using electrocoagulation (EC) method, Desalination 66 (1987) 353–364.
[42] M.C. Hernández, L. Barletta, M.B. Dogliotti, N. Russo, D. Fino, P. Spinelli, Heavy metal removal by means of electrocoagulation using aluminum electrodes for drinking water purification, J. Appl. Electrochem. 42 (9) (2012) 809–817.
[43] D.B. Wellner, S.J. Couperthwaite, G.J. Millar, The influence of coal seam water composition upon electrocoagulation performance prior to desalination, J. Environ. Chem. Eng. 6 (2) (2018) 1943–1956.
[44] H.I. Maarof, W.M.A.W. Daud, M.K. Aroua, Recent trends in removal and recovery of heavy metals from wastewater by electrochemical technologies, Rev. Chem. Eng. 33 (4) (2017) 359–386.
[45] H. Chow, A.L.T. Pham, Mitigating electrode fouling in electrocoagulation by means of polarity reversal: the effects of electrode type, current density, and polarity reversal frequency, Water Res. 197 (2021), 117074.
[46] D. Kim, R.J. Palacios, S. Ko, Characterization of sludge generated by electro-coagulation for the removal of heavy metals, Water Treat. 52 (4–6) (2014) 909–919.
[47] C. Comninellis, G. Chen, Electrochemistry for the Environment, Springer, 2010.
[48] T. Yehya, M. Chafi, W. Balla, C. Vial, A. Essadki, B. Gourich, Experimental analysis and modeling of denitrification using electrocoagulation process, Sep. Purif. Technol. 132 (2014) 644–654.
[49] D. Kumar, C. Sharma, Paper industry wastewater treatment by electro-coagulation and aspect of sludge management, J. Clean. Prod. 360 (2022), 131970.
[50] W. Xue, Y. Cui, Z. Liu, S. Yang, J. Li, X. Guo, Treatment of landfill leachate nanofiltration concentrate after ultrafiltration by electrochemically assisted heat activation of peroxydisulfate, Sep. Purif. Technol. 231 (2020), 115928.
[51] B. Zhou, Z. Yu, Q. Wei, H. Long, Y. Xie, Y. Wang, Electrochemical oxidation of biological pretreated and membrane separated landfill leachate concentrates on boron doped diamond anode, Appl. Surf. Sci. 377 (2016) 406–415.
[52] Y. Wang, X. Li, L. Zhen, H. Zhang, Y. Zhang, C. Wang, Electro-Fenton treatment of concentrates generated in nanofiltration of biologically pretreated landfill leachate, J. Hazard Mater. 229 (2012) 115–121.